Stable Salt Hydrate-based Thermal Energy Storage Materials

Yuzhan Li[1,2], Navin Kumar[2,7], Jason Hirschey[3], Damilola O. Akamo[2,4], Kai Li[2], Tugba Turnaoglu[2], Monojoy Goswami[5], Orlando Rios[6], Tim J. LaClair[2], Samuel Graham[3], Kyle R. Gluesenkamp[2]

1 School of Materials Science and Engineering, University of Science and Technology Beijing, Beijing 100081, China
2 Building and Transportation Sciences Division, Oak Ridge National Laboratory, Oak Ridge, Tennessee 37830, USA
3 Mechanical Engineering Department, Georgia Institute of Technology, Atlanta, Georgia 30332, USA
4 The Bredesen Center for Interdisciplinary Research and Graduate Education, University of Tennessee, Knoxville, TN, 37996, USA
5 Chemical Sciences Division, Oak Ridge National Laboratory, Oak Ridge, Tennessee 37830, USA
6 Materials Science and Engineering Department, University of Tennessee, Knoxville, Tennessee 37996, USA
7 Building Energy Efficiency Group, Gas Technology Institute, Des Plaines, Illinois 60018, USA

*Email of the corresponding author:
gluesenkampk@ornl.gov

Abstract

Heating and cooling systems in building infrastructure utilize conventional materials that account for a considerable amount of energy usage and waste. Phase change material (PCM) is considered a promising candidate for thermal energy storage that can improve energy efficiency in building systems. Here, a novel salt hydrate-based PCM composite with high energy storage capacity, relatively higher thermal conductivity, and excellent thermal cycling stability was designed and developed. The thermal cycling stability of the PCM composite was enhanced by using dextran sulfate sodium (DSS) salt as a polyelectrolyte additive, which significantly reduced the phase segregation of salt hydrate. The energy storage capacity and the thermal conductivity of the composite were enhanced by the addition of various graphitic materials along with Borax nucleator. A significant increase in thermal cycling stability was observed for the DSS-modified composite, with over 100 thermal cycles without degradation. The final PCM composite exhibited as much as 290% increase in energy storage capacity relative to the pure salt hydrate, and approximately 20% increase in thermal conductivity. In addition, the PCM composite developed can be produced at larger scale, and can potentially change the future of heating/cooling system in building infrastructure.

Keywords: phase change material; sodium sulfate decahydrate; phase separation; polyelectrolyte; thermal cycling

1. Introduction

Buildings utilize energy in a wide variety of ways, including heating, ventilation, and air conditioning. In the United States, residential and commercial buildings use 74% of the nation's electricity and account for 39% of all energy consumption.[1] The large amount of energy usage accompanies huge energy loss that necessitates developing novel emerging technologies for building infrastructure. Thermal energy storage (TES) is a promising technology to reduce the energy usage of buildings.[2, 3] Unlike renewable energy sources, such as solar, geothermal, and wind, which are variable and fluctuate strongly during the day and over different seasons of the year, TES provides a means of efficiently storing and extracting energy at specific time or seasons, thereby enabling the supply and demand of the thermal energy to be decoupled with time or space.[4] This allows buildings to take advantage of periods of more economical or more efficient energy supplies to shift peak electric loads and increase energy savings.

Latent heat storage is one of the most promising TES technologies for building applications because of its high storage density at nearly isothermal conditions.[5] Latent heat storage relies on the use of phase change materials (PCMs), such as paraffin waxes, fatty acids, salt hydrates and their eutectics.[6, 7] These materials can store large amounts of thermal energy as latent heat when changing from one phase to another under an isothermal condition. Although PCMs have been used in a range of small-scale thermal storage and temperature control applications for the last 3 decades, new approaches are continually being developed for large-scale applications, which have led to many technologies that enable improved energy efficiency at a low cost.[8-11] PCMs can provide thermal mass to dampen temperature extremes for any thermally cyclic system. This is important to thermally sensitive systems where large and sudden temperature swings are undesirable. Examples include the incorporation of PCMs into building envelopes, clothing and textiles, electronics, batteries, solar photovoltaics, and refrigeration systems.[12-15]

Paraffins are the most utilized PCM today. However, with a typical material cost of 20-40 $/kWh, they are too expensive for most building applications.[16] On the contrary, salt hydrates are promising candidates because of their low cost and high thermal energy storage density.[17-19] For example, sodium sulfate decahydrate, $Na_2SO_4 \cdot 10H_2O$ (SSD), has been identified as one of the most promising salt hydrates for building applications due to its low cost (1.60 $/kWh), high energy storage capacity (254 J/g), and moderate melting temperature (32.4 °C).[20, 21] Nonetheless, the widespread use of SSD as a PCM has been prevented by the material's phase separation behavior upon thermal cycling, which results in significant degradation of thermal energy storage capacity over extended freeze/melt cycles.[22, 23] The phase separation of SSD originates from its incongruent melting behavior, which is illustrated in Figure 1. When SSD undergoes melting, the water molecules from the crystalline SSD phase are released to the liquid water phase. The remaining anhydrous sodium sulfate (SS) salt cannot be fully dissolved in the water, resulting in a saturated salt solution with undissolved salt particles (Figures 1b and 1f). Due to the difference in density between the salt solution and the solid salt, the high-density SS particles tend to precipitate (settle) to the bottom (Figures 1c and 1g) resulting in a phase-separated mixture. Consequently, the phase-separated mixture cannot be fully recovered to SSD upon freezing (Figures 1d and 1h). As such, the latent heat associated with the freezing process is less than that associated with the previous melting process since less material undergoes the freezing phase transition. This represents a degradation of thermal energy storage capacity of the material upon thermal cycling. Furthermore, repeated thermal cycling can exacerbate the degradation as phase

separation continues. Therefore, reducing the phase separation behavior of SSD is crucial for enabling its widespread use as a PCM for building applications.[24]

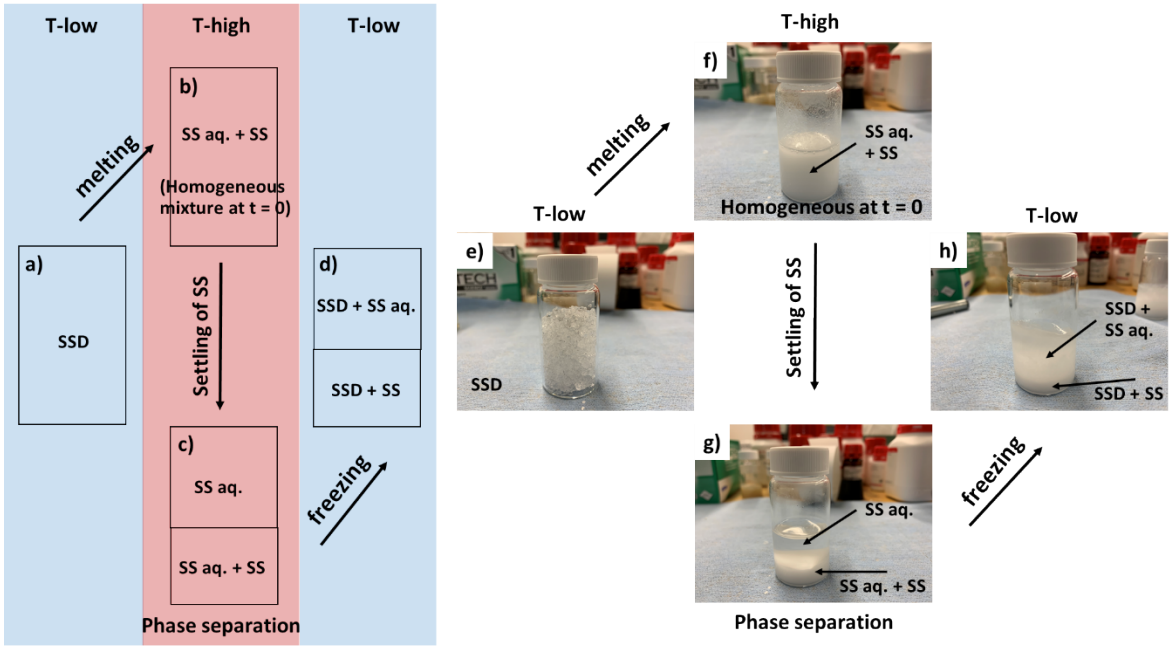

Figure 1. Thermal cycling behavior of SSD. (a-d) Illustration of the phase separation behavior of SSD upon thermal cycling and (e-h) visualization of the phase separation behavior of SSD upon thermal cycling.

Prior works have shown that the use of a thickening agent is an easy and effective way to mitigate the phase separation of SSD.[25] A wide variety of thickening agents have been tested and investigated, including attapulgite clay, carboxymethyl cellulose, sodium alginate, polyacrylamide, and micro/nano fibrillated cellulose.[26-29] Generally, these additives increase viscosity of the salt solution, reducing the settling effect of the salt particles. However, the efficacy of thickening is often affected by the high ionic strength of the saturated salt solution, which disrupts hydrogen bonding between water molecules and the hydrophilic groups of the thickening agent.[30] Another widely used method to tackle the phase separation problem of SSD is encapsulation, in which the salt hydrate is enclosed by a shell material, such as silicon oxide, or is trapped in a porous polymer network, such as polyurethane.[31-34] However, these methods often require relatively high-cost, complex materials processing that undermines the price advantage of SSD, and hence is undesirable in low-cost materials design and applications. Moreover, the thermal energy storage capacity of these encapsulated SSD is usually lower than that of thickened SSD due to the higher weight percentage of the non-active materials from the shell or the porous network.

In this work, a novel strategy was developed and validated to reduce the phase segregation of SSD by using a water soluble, negatively charged polysaccharide, dextran sulfate sodium (DSS), as an anionic polyelectrolyte additive. In nanotechnology applications, polyelectrolytes are often used as additives to stabilize nanoparticle emulsions in aqueous or organic solvents through steric stabilization and/or electrostatic stabilization.[35, 36] However, the use of this method to stabilize the undissolved, suspended sodium sulfate (SS) particles during the solid-to-liquid (melting) and

liquid-to-solid (freezing) phase transitions of SSD to prevent phase separation has not yet been explored. Therefore, the present study, focusing on stabilization of SSD salt hydrate during phase transition, is unique and shows promising performance for TES applications. Contrary to previous studies, DSS is not used as a thickening agent; instead, it acts as an additive that significantly reduces phase segregation of SSD during repeated thermal cycling by reducing the rate of precipitation of the salt particles. In addition to DSS, the PCM composite also contains sodium tetraborate decahydrate (Borax) to expedite nucleation and reduce supercooling, and several different types of graphitic fillers to improve thermal conductivity. The investigation of the freezing and melting processes of SSD with different loadings of DSS indicates that the reduced salt domain sizes and increased electrostatic interactions between the salt particles are responsible for the improved thermal cycling stability. It is also demonstrated that when combined with the traditional thickening method, large scale SSD-based PCM samples can be prepared, which exhibit excellent thermal cycling performance, energy storage capacity and good thermal conductivity that can have great potential as TES materials for building applications.

2. Experimental

2.1 Materials and sample preparation

Sodium sulfate decahydrate (SSD) salt hydrate, dextran sulfate sodium (DSS) polyelectrolyte, and sodium tetraborate decahydrate ($Na_2B_4O_7 \cdot 10H_2O$, Borax) were purchased from Sigma-Aldrich, expanded graphite (GRAFOIL, TG-855A) and jet milled expanded graphite (GRAFOIL, TG-679) were supplied by NeoGraf Solutions, LLC. Graphite flakes with average particle sizes of 10 and 44 μm were purchased from Alfa Aesar. Graphene Nanoplatelets (xGnP, Grade M) with an average particle diameter of 5 μm was obtained from XG Sciences Inc. All materials were used without further purification. The theoretical energy storage capacity and melting temperature of pure SSD were 254 J/g and 32.4 °C respectively.

Small-scale samples were prepared by mixing SSD and DSS in different weight ratios (100:0, 100:0.5, and 100:5) to study the effect of DSS and were labeled PCM-0, PCM-0.5, and PCM-5, respectively. During the sample preparation, SSD and DSS were sealed in a glass vial and were homogenized in a heated sonication bath of 50°C for 30 min. Then, the mixture was used for different characterizations.

Large-scale PCM composite samples were prepared using a fixed SSD and DSS weight ratio of 100:5. In the preparation of PCM composites, Borax was added as a nucleator to reduce supercooling. Graphite fillers were added to improve thermal conductivity and to increase the viscosity of the composites to reduce phase separation. A detailed preparation procedure is shown in Figure S1 in supporting information.

2.2 Characterization

Small-scale thermal cycling stability tests were carried out using a differential scanning calorimeter (DSC 2500, TA Instruments) under a nitrogen purge of 50 mL/min. The sample (20-30 mg) was hermetically sealed in an aluminum DSC pan and was thermally cycled between -50 °C to 60 °C with a ramp rate of 5 °C/min. The heating scans were used to determine the melting point and the melting enthalpy of the PCM samples.

Large-scale thermal cycling stability of the PCM samples was investigated using a Temperature-History (T-H) method.[37] In the T-H experiment, the sample (15-20 g) was loaded into a borosilicate glass tube (length of 190 mm and diameter of 10 mm). The glass tube was sealed

with a rubber stopper with a center hole for thermocouple insert. A 1/16" sheathed T-type thermocouple was inserted into the PCM sample. A reference borosilicate glass tube was prepared with water as a reference medium. The glass tubes were placed in a bench-top environmental temperature chamber (ESPEC SH-242) and thermally cycled between 15°C to 45 °C at a ramp rate of 5°C/min. The temperature in the chamber was measured with 1/16" sheathed T-type thermocouple. The temperature of the chamber, reference and PCM samples were recorded using a National Instruments cDAQ 9214 data acquisition system at a frequency of 0.2 HZ (5 sec/sample). The recorded temperature profile was used to investigate the melting and freezing behavior of the PCM samples. The phase change temperature, latent heat, and degree of supercooling were analyzed as reported in previous work from the literature.[38]

Viscosity tests were carried out using a parallel plate rheometer (Discovery HR, TA Instruments). The PCM sample (in the molten form) was sandwiched between two stainless steel plates with a gap of 1 mm, and a logarithmic sweep of shear rate from 1 to 100 1/s was performed at 40 °C.

Optical images of the PCM samples were collected using an Olympus BX50 optical microscope. In this experiment, the PCM samples were melted in a glass vial. Then, a few drops of the molten PCM samples were sandwiched between two glass slides. The optical images were taken at room temperature while the PCM samples were in a supercooled state. Borax was not used in this experiment to prevent crystallization of the PCM samples at room temperature.

Zeta potential measurements were carried out on pristine sodium sulfate, pristine DSS, and PCM-5 using capillary electrophoresis (ZetaPALS, Brookhaven Instruments) to investigate the surface charge. The solid particles were suspended in 1 mM KNO_3 at dilute concentrations (~10^{-6}). The pH of the suspensions was adjusted over a broad range (2-10) using stock solutions of 1 M HNO_3 and 1 M NH_4OH. The suspensions were equilibrated for 24 hours before measurements.

Small-angle X-ray scattering (SAXS) measurements were carried out on a Xenocs Xeuss 3.0 instrument equipped with D2+ MetalJet X-ray source (Ga Kα, λ = 1.341 Å). The PCM samples were loaded in a capillary tube, which was then sealed with epoxy resins. SAXS measurements were performed at two different positions (top and bottom) of the tube to investigate the settling behavior of the sodium sulfate salt particles. The scattered beam was recorded on a Dectris Eiger 2R 4M hybrid photon counting detector with a pixel dimension of 75 × 75 μm^2. The collected 2-dimensional (2D) SAXS images were circularly averaged and expressed as intensity versus q, where $q = (4\pi \sin\theta)/\lambda$ after subtraction of background scattering. The SAXS images were collected at the sample-to-detector distance of 1800 mm.

X-ray diffraction (XRD) was performed using PANalytical X'Pert Pro to determine the composition of the PCM samples. XRD data were collected at a scan rate of 0.2°/min over a 2θ range of 10° to 50°. Rietveld refinement of the XRD data was performed using HighScore Plus (Malvern Panalytical) to determine phase fraction (hydrate and salt) of the PCM samples.

3. Results and discussion

3.1 Effect of DSS

In general, smooth phase transition from solid to liquid state is essential for PCM to be widely adopted for TES applications. However, pure SSD phase separates during melting, which results in precipitation of undissolved sodium sulfate (SS) particles. Therefore, strategies that promote the formation of a homogenous suspension of the undissolved SS particles can mitigate

phase separation and improve thermal cycling stability of SSD. Polyelectrolytes are extensively used in colloidal science to enclose partially charged nanoparticles to ascertain stable homogeneous suspension by electrostatic stabilization. However, the same has not been explored to stabilize SS particles in salt hydrate PCMs. In this work, DSS was used as a polyelectrolyte to promote the formation a stable homogeneous suspension of the SSD salt hydrate.

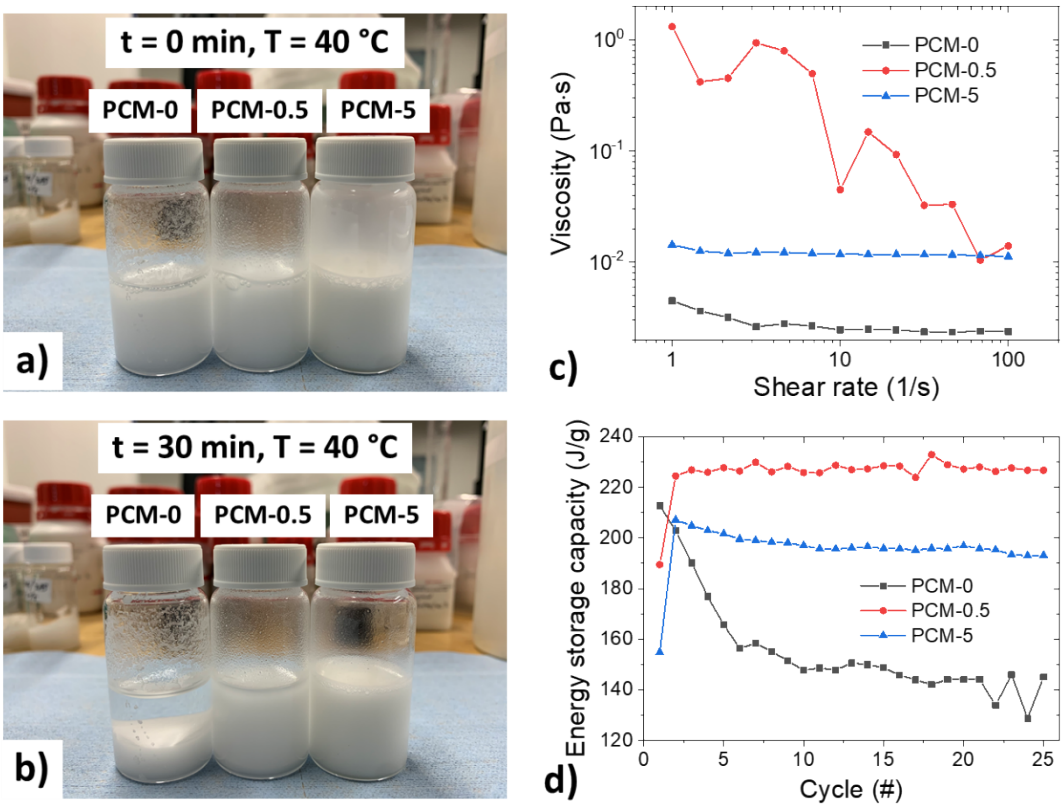

Figure 2. Effect of DSS on the settling rate of SS particles and on the thermal cycling stability of PCM samples. a) Photo of the molten PCM samples before particle settling showing homogeneous mixture. (b) Photo of the molten PCM samples after 30 min of settling. PCM-0, PCM-0.5 and PCM-5 represents 0, 0.5 and 5 wt% of DSS, respectively. (c) Viscosity measurements of the molten PCM samples. (d) Thermal cycling stability of the PCM samples determined using small-scale DSC tests. Color legends representing the different samples are shown in figures (c) and (d).

When DSS is dissolved in aqueous solutions, the sodium cations disassociate from the polyelectrolyte, resulting in negatively charged dextran sulfate (DS) polyanions. In Figure 2a and 2b, the cloudy homogeneous solution can be observed in PCM-0.5 and PCM-5 samples, representing the presence of DS polyanions effectively reduced the settling rate of the SS particles and promoted the formation of a homogeneous suspension. The undissolved SS particles in PCM-0 quickly (less than 3 min) settled to the bottom of the glass vial, whereas the SS particles in PCM-0.5 and PCM-5 remained suspended even after 30 minutes (long-term stability is discussed later). Interestingly, the viscosity of the DS-modified PCM samples only exhibited a small increase compared to the unmodified PCM sample (black curve in Figure 2c). The small increase in viscosity further confirms our hypothesis that the stabilization of the SS particles was not achieved

through a physical trapping mechanism as it happens in the traditional thickening method, such as those observed in sodium polyacrylate-modified or carboxymethyl cellulose-modified SSD.[39, 40] Instead, the DS polyanions act as a barrier, covering the SS particles and resulting in a strong electrostatic interaction between the DS-covered SS particles. This reduced the setting rate of the SS particles, thereby giving rise to improved thermal cycling stability of the DS-modified PCM samples, as shown in Figure 2d. In contrast, the unmodified PCM-0 sample exhibited a significant loss of energy storage capacity over the first few heating/cooling cycles, which also resulted in a change of melt peak temperature (Figure S2 in supporting information). It is noteworthy that the PCM-0.5 sample did not achieve equilibration with only 0.5 wt% DSS, which was not enough to encapsulate majority of the SS particles that resulted in a non-equilibrium mixture of SS and DS, and hence it showed inconsistent viscosity behavior.

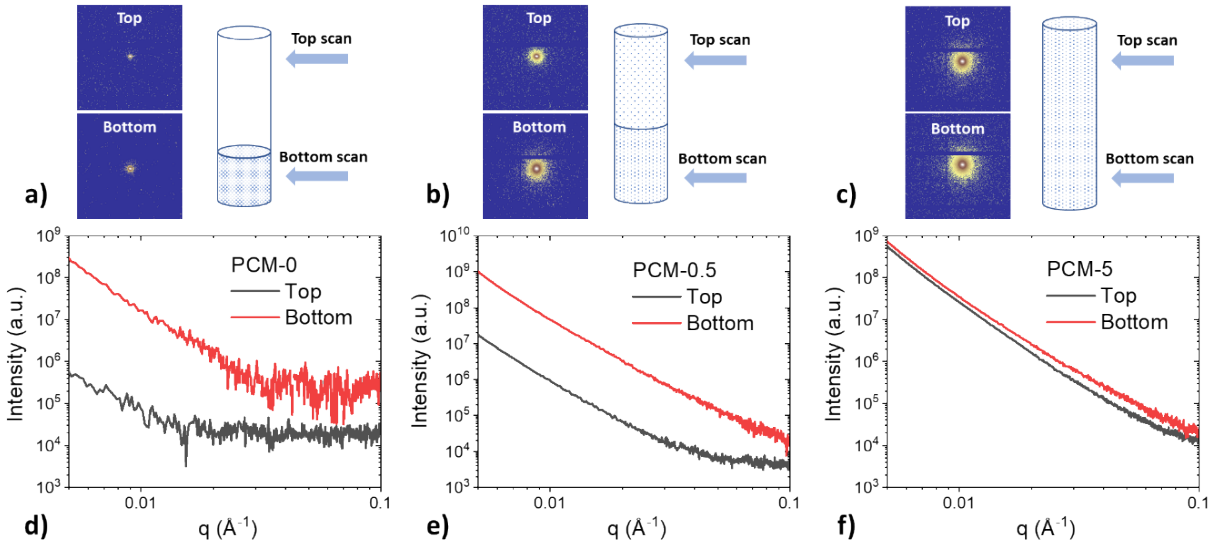

Figure 3. Effect of DSS on the homogeneity of PCM samples. (a-c) 2D SAXS patterns collected at the top and bottom sections of capillary tubes containing PCM-0, PCM-0.5, and PCM-5, respectively. (d-f) Integrated 1D SAXS profiles of PCM-0, PCM-0.5, and PCM-5, respectively.

The effect of DS polyanions on the homogeneity of the molten PCM samples was investigated by structural analysis using small-angle X-ray scattering (SAXS), as shown in Figures 3a to 3c. Each PCM sample was placed in a capillary tube on the SAXS sample holder, two scans were performed: one at the top section and the other one at the bottom section of the capillary tube. The 2D patterns, Figure 3(a), (b) and (c), were integrated isotopically to generate 1D intensity profiles, Figure (d), (e) and (f) respectively. Since the incident X-rays were scattered by the undissolved SS particles in the molten PCM samples, they contain the structural information of SS particle dispersion that can explain sample homogeneity. The PCM-0 exhibited weak SAXS signals at both scattering locations. This was attributed to the quick settlement of the SS particles, which is schematically illustrated in Figure 3a (right). The weak SAXS signal of the top scan was caused by the absence of scattering objects (SS particles), whereas the weak SAXS signal of the bottom scan was caused by closely packed SS particles which blocked most of the incident X-rays. With the addition of DSS, the settling rate of the SS particles was reduced, resulting in a more homogenous suspension all along the capillary tube with improved SAXS signals at top and bottom. As shown in Figure 3b, the diffuse halo around the bright center beam for PCM-0.5

indicated the scattered X-rays by the suspended SS particles. However, there exists a difference in scattering intensity between the top scan and the bottom scan, implying that the sample was not entirely homogenous along the capillary tube (Figure 3e). It may be due to addition of only a tiny (0.5 wt%) amount of DSS that did not equilibrate the PCM sample. Increasing the concentration of DSS increased the number of DS polyanions and significantly improved sample homogeneity. As shown in Figures 3c and 3f, the 2D patterns and the integrated 1D profiles of the top scan and the bottom scan for PCM-5 are essentially the same, indicating highly homogeneous PCM sample from top to bottom of the capillary. Again, this was attributed to the reduced precipitation/settling rate of the SS particles due to the presence of DS polyanions.

3.2 Stabilization mechanism

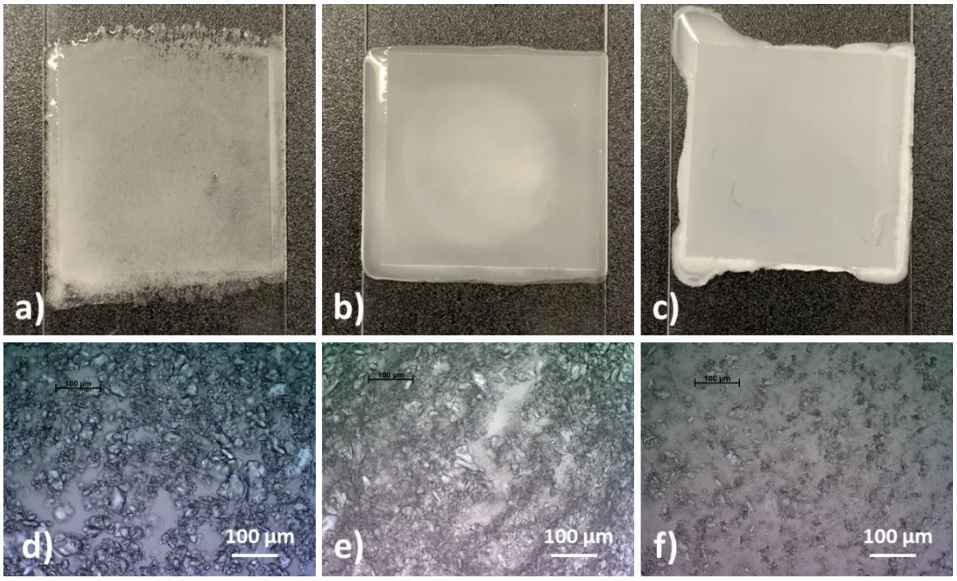

Figure 4. Effect of DSS on the size of suspended sodium sulfate particles in the molten PCM samples. (a-c) Photos of sandwiched molten PCM samples. (d-f) Optical images of sandwiched molten PCM samples under a magnification of 200x. From left to right: PCM-0, PCM-0.5, and PCM-5.

Optical microscopy was used to characterize the suspended SS particles in the molten PCM samples. In Figure 4, the optical images of the bare PCM sample and DSS-added samples showed significant difference in the optical properties. The sandwiched PCM-0 suspension showed void in the sample and was not uniform (Figure 4a). Large SS particles and aggregates (dark areas in Figure 4d) were observed under a 200x higher magnification (Figure 4d). The sandwiched suspension became increasingly uniform with the addition of DS polyanions, as shown in Figures 4b and 4c. Moreover, a reduction of aggregate sizes of SS particles was observed for PCM-0.5 and PCM-5 (Figures 4e and 4f). This indicates that the DS polyanions acted as a physical barrier encapsulating small SS particles, thereby separating undissolved SS particles, and preventing them from forming large aggregates that quickly settle. The reduced size of suspended SS particles/aggregates and the resulting sample uniformity were responsible for the high thermal cycling stability of the PCM samples with DSS as observed in Figure 1d.

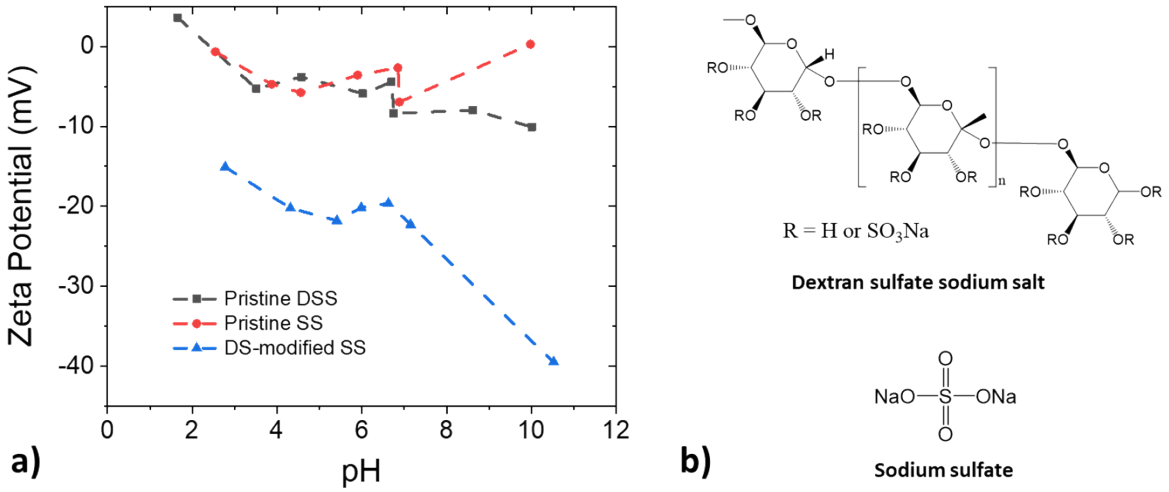

Figure 5. a) Zeta potential measurements of pristine DSS, pristine SS particles, and DS-modified SS particles. The dashed-lines are guide to the eye. b) Chemical structure of dextran sulfate sodium salt and anhydrous sodium sulfate.

The stabilization mechanism was further investigated by comparing the Zeta potentials of pristine DSS, pristine SS, and DS-modified SS particles, and the results are shown in Figure 5a. As mentioned previously, DSS is a neutral polyelectrolyte salt, which is reflected by the near-zero Zeta potential (black curve) values across the investigated pH conditions. Similar behavior was observed for the pristine SS particles (red curve), which is also a neutral salt. In contrast, the DS-modified SS particles exhibited large negative Zeta potential values (blue curve). This indicated that the SS particles were covered by a layer of DS polyanions, resulting a negatively charged surface. The DS layer introduced an electrostatic force between the encapsulated SS particles, thereby forming a stable SS suspension. This reduced the settling rate and phase separation behavior, which is schematically illustrated in Figure 6a. This is evident from the relatively flat (around -20mV) zeta potential extending up to neutral pH ≤ 7.0 (acidic regime). However, it is noteworthy that the suspended nature of the SS particles in the presence of DSS particles was not sufficient to totally eliminate the flocculation after a long time. As shown in Figure 6b, a notable phase separation between SS particles and SS aqueous solution was observed after 24 hours of settlement for PCM-5 (rightmost capillary tube). Nevertheless, the degree of phase separation was significantly lower than that of PCM-0 and PCM-0.5.

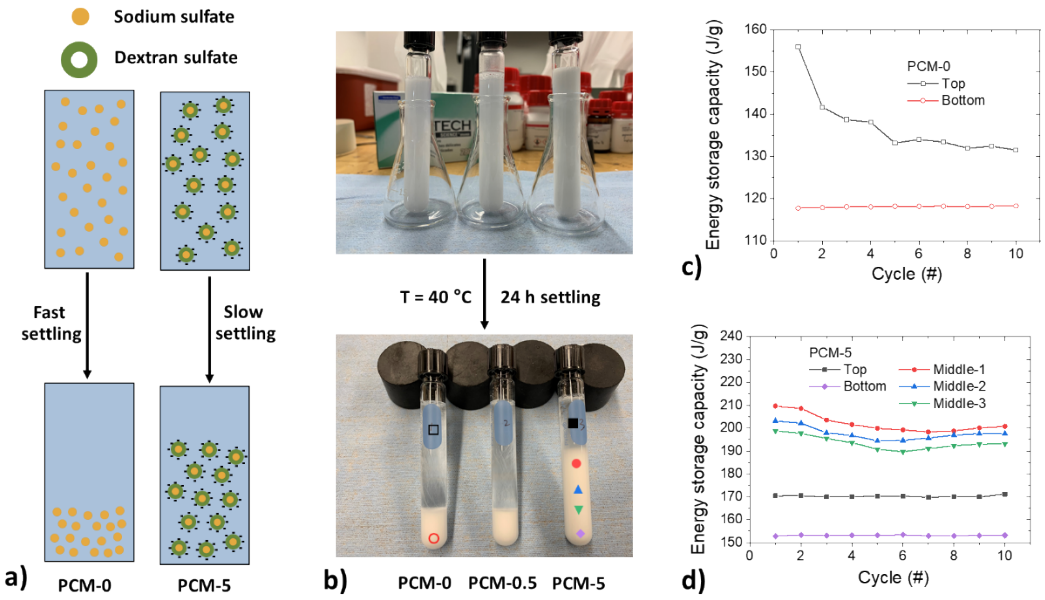

Figure 6. (a) Schematic illustration of the stabilization mechanism of DS-modified SS particles. (b) Effect of DSS on the phase separation of the PCM samples as observed through photographed samples. (c) Energy storage capacities of the top and bottom phase separated PCM-0. (d) Energy storage capacities of the separated phases of PCM-5.

To determine the energy storage capacity of the separated phases, samples were collected at the top and bottom from the glass tube (indicated by the black and red symbols in Figure 6b) and were thermally cycled in DSC. As shown in Figure 6c, the samples collected from the top (open black square) and the bottom (open red circle) of PCM-0 exhibited energy storage capacities of 131.5 and 118.2 J/g, respectively. Both are considerably lower than the full energy storage capacity of SSD. As illustrated in Figure 1h, the top clear section consisted of aqueous solution of SSD and SS, and the bottom opaque section consisted of concentrated SSD and SS particles. If there were no phase separation, the solution would look homogeneous, i.e., the degree of phase separation determined the concentration of SSD in both sections. This is reflected by the distinct thermal cycling behavior of PCM-5. As shown in Figure 6d, the samples collected from the top (closed black square) and the bottom (closed purple diamond) of PCM-5 exhibited energy storage capacities of 171.1 and 153.2 J/g, respectively. Both values are higher than those observed for the PCM-0 samples, indicating higher concentrations of SSD in both sections due to the reduced phase separation. More importantly, the samples collected from the middle section of PCM-5 exhibited high energy storage capacities about 200 J/g, possibly due to the well-suspended SS particles. This implies that the stabilization of the SS particles is the key to realize high thermal cycling stability of SSD. In order to confirm the composition of the collected samples from PCM-5, powder X-ray diffraction (XRD) was performed and the spectra were analyzed using the Rietveld refinement method (Supplementary Figure S3). The weight percentages of SSD and SS for the samples collected from the middle and bottom sections are summarized in Table 1. Significantly higher concentrations of SSD were detected for the samples collected from the middle sections, which are responsible for their high energy storage capacities. In addition, a slight decrease of SSD concentration was observed as the sample location moved toward to the bottom, reflecting the slow

settling process of DS-modified SS suspended particles. This indicates that additional stabilization methods are required to further reduce the settling of SS particles.

Table 1. Composition of samples collected at different locations of the phase separated PCM-5 and comparison between the calculated energy storage capacity by XRD and the measured value by DSC.

Sample location	SSD (wt.%)	SS (wt.%)	Calculated energy storage capacity by XRD (J/g)	Measured energy storage capacity by DSC (J/g)
Middle-1	94.2	5.8	207.2	209.6
Middle-2	88.9	11.1	195.6	203.2
Middle-3	87.5	12.5	192.5	198.7
Bottom	63.8	36.2	140.4	152.8

3.3 PCM composites

While phase separation is the key issue affecting widespread use of SSD as a PCM, the low thermal conductivity and high degree of supercooling are two other important limiting factors of salt hydrate-based PCMs.[38] Based on the promising results of PCM-5, composites of PCM-5 were prepared with expanded graphite (EG) to improve thermal conductivity and sodium tetraborate decahydrate ($Na_2B_4O_7 \cdot 10H_2O$, Borax) to reduce the degree of supercooling. The added EG also served as a thickening agent, increasing viscosity and further reducing the phase separation of the PCM composites. Three other types of graphite variations were used to prepare the samples, milled expanded graphite (MEG), graphite flakes (GF) of sizes 10 and 44 μm, and graphene nanoplatelets (GNP). Table 2 summarizes the composition, energy storage capacities, and thermal conductivity of the developed PCM composites. It is important to mention here that the energy storage capacities were determined using a temperature-history (T-H) method, which allowed for the evaluation of thermal cycling stability of PCM samples with larger quantities (15-20 g). The testing conditions in the T-H method are similar to the environments that the PCM samples are likely to experience in real applications, reflecting the performance of the samples in reality. Figure 7a compares the thermal cycling behavior of the PCM composites with EG and different amounts of DSS evaluated using the T-H method. Pristine SSD (sample 1) exhibited a sharp decrease in energy storage capacity in the first 40 cycles due to phase separation. The addition of EG (sample 2, red line) improved thermal cycling stability, however, the energy storage capacity was low, implying that physical thickening by EG alone was not sufficient to eliminate phase separation and enhance energy storage capacity. The energy storage capacities increased significantly with the addition of DSS (sample 3-5) to the PCM composite. Furthermore, the PCM samples exhibited improved thermal cycling stability as can be observed from the plateaued energy storage capacity curve extending up to 100 cycles. The PCM composite with 5 wt% DSS loading showed a slight decrease of energy storage capacity from 155.8 J/g to 151.3 J/g over 100 cycles. This excellent stability of the PCM composite is highly desirable material property for TES in building applications. While energy storage capacity and stability of the composite with DSS additive increases significantly, we have not observed the same for thermal conductivity. Table 2 shows that the thermal conductivity lies between 3.6 to 4.3 $Wm^{-1}K^{-1}$ from Sample 2 to Sample 5. While the 5 wt% DSS sample shows ~20% increase in thermal conductivity, this is insignificant compared to the increase in thermal conductivity due to the addition of EG. As discussed earlier, DSS helps in encapsulating the small SS particles thus stabilizing the suspension, it does not help

in enhancing thermal conductivity. However, EG helps increase the thermal conductivity when composited with pristine SSD as is evident from Table 2.

Table 2. Composition, energy storage capacity, and thermal conductivity of PCM composites

Sample	Composition	Weight ratio	Energy storage capacity at the 100th cycle (J/g)	Thermal conductivity ($W \cdot m^{-1} \cdot K^{-1}$)
1	SSD	100	46.2	N/A
2	SSD/EG/Borax	100/15/5	67.7	3.6±0.3
3	SSD/EG/DSS/Borax	100/15/1/5	92.9	3.8±0.2
4	SSD/EG/DSS/Borax	100/15/2/5	142.9	3.9±0.2
5	SSD/EG/DSS/Borax	100/15/5/5	151.3	4.3±0.2
6	SSD/MEG/DSS/Borax	100/15/5/5	166.6	4.5±0.5
7	SSD/GF10/DSS/Borax	100/15/5/5	169.1	2.8±0.2
8	SSD/GF44/DSS/Borax	100/15/5/5	142.9	2.9±0.3
9	SSD/GNP/DSS/Borax	100/3/5/5	178.2	N/A

N/A – Not available

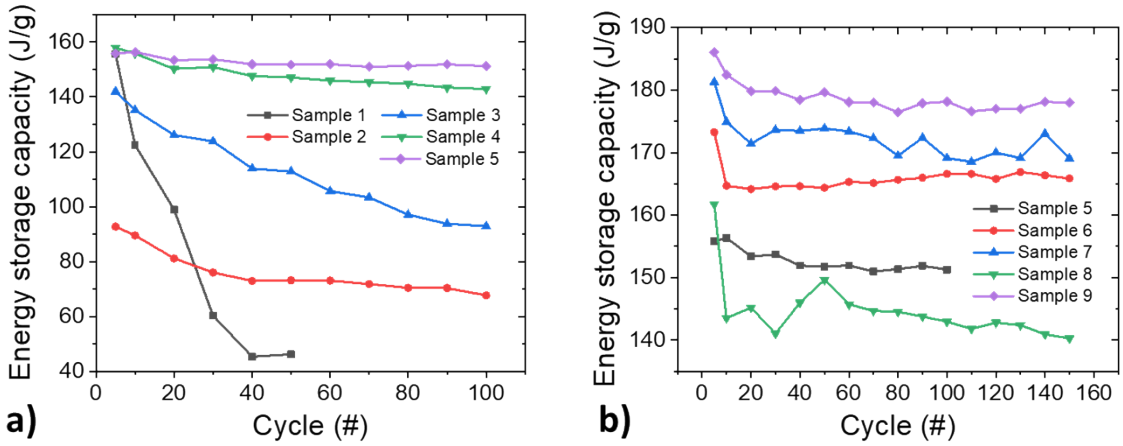

Figure 7. Thermal cycling stability and energy storage capacity of PCM composites. (a) Effect of different amounts of DSS. (b) Effect of different types of carbon fillers.

To this end, different types of carbon fillers in the PCM composite were examined, including milled EG (MEG), graphite flakes (GF10 and GF44), and graphene nanoplatelets (GNP). As shown in Figure 7b, all the PCM composites exhibited an initial drop of energy storage capacity in the first 10 cycles, which was attributed to the presence of voids during the sample loading process. During first 10-15 melting/freezing cycles, these voids were gradually filled by the PCM composites, and the thermal cycling performance became stable. In Figure 7b, Sample 5 to Sample 8 contained DSS, which is crucial for reducing the phase separation during the processing step and is important for the PCM composites to maintain high initial energy storage capacities. Interestingly, the type of carbon fillers showed a strong influence on the energy storage capacity of the PCM composites. We hypothesize that the reduction of energy storage capacity for different fillers was an artifact of the filler sizes. It was observed that fillers with larger sizes, such as EG (sample 5) and GF44 (sample 8), resulted in lower energy storage capacities. EG has worm-like

structures with sizes in the micrometer scale, whereas GF44 has an average particle size of 44 µm. This may be due to the small number of voids present in the loosely packed PCM filled with larger size filler particles reducing their thickening efficiency, and therefore these PCM composites had relatively low energy storage capacities. In contrast, the PCM composites prepared using MEG (sample 6), GF-10 (sample 7), and GNP (sample 9), showed stable and higher energy storage capacities. The average particle size of MEG, GF-10, and GNP was 20 µm, 10 µm, and 5 µm, respectively, much smaller than EG and GF44 samples. The smaller size of the fillers can pack better to reduce voids and hence can exhibit a greater thickening effect. This coupled with the stabilizing effects of DSS, result in PCM composites with excellent thermal cycling performance with higher energy storage capacity. However, it is noteworthy that the morphology of the fillers greatly influenced the thermal conductivity of the PCM composites (Table 2). The thermal conductivity of Sample 5 and 6 (4.3 and 4.5 $Wm^{-1}K^{-2}$) shows relatively higher values compared to the thermal conductivities of sample 7 and 8 (2.8 and 2.9 $Wm^{-1}K^{-2}$). While EG/MEG significantly increases the thermal conductivity in general, we cannot explain with certainty a drop of > 30% in thermal conductivity due to the addition of graphite flakes, this requires further investigation in future.

3.4 Cost analysis

The major cost for thermal energy storage system comes from the raw thermal storage material itself. The cost of the raw thermal storage material is directly related to the energy density (kWh/m^3) and the power density (W/m^3). Hirschey et al. summarized and provided detailed materials cost ($/kWh) analysis of various classes of PCMs with phase change between 0-65°C, with many salt hydrates with low material costs, high latent heat of fusion, and high densities, leading to favorable volumetric storage density and low energy costs of 50–130 kWh/m^3 and 0.90–40$/kWh, respectively.[16] One of the lowest cost and high energy density material in the temperature range of 25 -35°C was SSD (< $0.09/kg), but it suffered from incongruent melting, supercooling and low thermal conductivity.[18] In this work, these issues were mitigated and the cost of the SSD-based composite was computed. The DSS cost ranged from $10/kg to $100/kg, therefore the cost of the DSS had a major impact on the overall cost of the composite. The minimum cost of the composite was $18.13/kWh and maximum cost was $116.31/kWh.

4. Conclusions

In this study, a novel materials design strategy was developed to improve the physical and chemical properties of SSD for its application as a PCM. A polyelectrolyte, dextran sulfate sodium (DSS) salt was used as an additive to reduce phase separation by encapsulating small SS particles. These suspended SS particles enclosed inside of the DS polyanions, due to strong electrostatic interactions, significantly reduce the precipitation/settling rate of SS particles during melting. Contrary to previous experiments where thickening agents were used, DSS did not serve as thickening agent, instead, it serves as a stabilizing additive that enhanced thermal cycling stability as well as energy storage capacity. Further investigation of the freezing and melting processes of SSD with different loadings of DSS reveals that the reduced sizes and increased electrostatic interactions between the SS particles led to the formation of a stable and homogeneous suspension, thus improving thermal cycling stability. It is also demonstrated that when combined with the traditional thickener and different types of graphite, both energy storage capacity and thermal conductivity can be enhanced. These stable SSD-based PCM composites can be prepared at a large

scale, which exhibited excellent thermal cycling performance with enhanced thermal conductivity and reduced degree of supercooling. The novel PCM composite material developed here promises great potential for heating and cooling in application in building infrastructure. Furthermore, the technique and strategy highlighted could be utilized to expedite to enhancement the performance of other incongruently melting salt hydrates and improve throughput of these materials to the market.

Acknowledgements

This work was sponsored by the U.S. Department of Energy's (DOE) Building Technologies Office under Contract No. DE-AC05-00OR22725 with UT-Battelle, LLC. The authors would like to acknowledge Mr. Sven Mumme from the U.S. Department of Energy Building Technologies Office. SAXS data were measured on the Xeuss 3 SAXS/WAXS instrument via the ORNL instrumentation pool and the data were analyzed at the Center for Nanophase Materials Sciences (CNMS) which is a U.S. Department of Energy, Office of Science User Facility. The authors thank Dr. Beth Armstrong at ORNL for assistance in the Zeta potential measurements and Dr. Jong K. Keum for assistance in the SAXS/WAXS measurements.

Conflicts of Interest

The authors declare no conflict of interest.

References

[1] Buildings, Emerging Technologies. https://www.energy.gov/eere/buildings/emerging-technologies (accessed 09/06/2021).
[2] Soares N, Costa JJ, Gaspar AR, Santos P. Review of passive PCM latent heat thermal energy storage systems towards buildings' energy efficiency. Energy and Buildings. 2013;59:82-103.
[3] da Cunha JP, Eames P. Thermal energy storage for low and medium temperature applications using phase change materials - A review. Appl Energy. 2016;177:227-38.
[4] Kenisarin M, Mahkamov K. Passive thermal control in residential buildings using phase change materials. Renew Sust Energ Rev. 2016;55:371-98.
[5] Agyenim F, Hewitt N, Eames P, Smyth M. A review of materials, heat transfer and phase change problem formulation for latent heat thermal energy storage systems (LHTESS). Renew Sust Energ Rev. 2010;14(2):615-28.
[6] Zhang N, Yuan YP, Cao XL, Du YX, Zhang ZL, Gui YW. Latent Heat Thermal Energy Storage Systems with Solid-Liquid Phase Change Materials: A Review. Adv Eng Mater. 2018;20(6):30.
[7] Pielichowska K, Pielichowski K. Phase change materials for thermal energy storage. Prog Mater Sci. 2014;65:67-123.
[8] Vadiee A, Martin V. Thermal energy storage strategies for effective closed greenhouse design. Appl Energy. 2013;109:337-43.
[9] Diaconu BM, Cruceru M. Novel concept of composite phase change material wall system for year-round thermal energy savings. Energy and Buildings. 2010;42(10):1759-72.
[10] Entrop AG, Brouwers HJH, Reinders A. Experimental research on the use of micro-encapsulated Phase Change Materials to store solar energy in concrete floors and to save energy in Dutch houses. Sol Energy. 2011;85(5):1007-20.

[11] Kuznik F, Virgone J, Johannes K. In-situ study of thermal comfort enhancement in a renovated building equipped with phase change material wallboard. Renew Energy. 2011;36(5):1458-62.
[12] Zhou D, Zhao CY, Tian Y. Review on thermal energy storage with phase change materials (PCMs) in building applications. Appl Energy. 2012;92:593-605.
[13] Mondal S. Phase change materials for smart textiles - An overview. Appl Therm Eng. 2008;28(11-12):1536-50.
[14] Khan MMA, Saidur R, Al-Sulaiman FA. A review for phase change materials (PCMs) in solar absorption refrigeration systems. Renew Sust Energ Rev. 2017;76:105-37.
[15] Kandasamy R, Wang XQ, Mujunidar AS. Application of phase change materials in thermal management of electronics. Appl Therm Eng. 2007;27(17-18):2822-32.
[16] Hirschey JR KN, Turnaoglu T, Gluesenkamp KR, Graham S. Review of Low-Cost Organic and Inorganic Phase Change Materials with Phase Change Temperature between 0°C and 65°C. In: Proceedings of 6th International High Performance Buildings Conference. West Lafayette, Indiana, Conference, Conference 2021.
[17] Xie N, Huang ZW, Luo ZG, Gao XN, Fang YT, Zhang ZG. Inorganic Salt Hydrate for Thermal Energy Storage. Appl Sci-Basel. 2017;7(12):18.
[18] Kumar N, Hirschey J, LaClair TJ, Gluesenkamp KR, Graham S. Review of stability and thermal conductivity enhancements for salt hydrates. J Energy Storage. 2019;24:15.
[19] Kenisarin M, Mahkamov K. Salt hydrates as latent heat storage materials:Thermophysical properties and costs. Sol Energy Mater Sol Cells. 2016;145:255-86.
[20] Marks SB. The effect of crystal size on the thermal energy storage capacity of thickened Glauber's salt. Sol Energy. 1983;30(1):45-9.
[21] Marks S. An investigation of the thermal energy storage capacity of Glauber's salt with respect to thermal cycling. Sol Energy. 1980;25(3):255-8.
[22] Mohamed SA, Al-Sulaiman FA, Ibrahim NI, Zahir MH, Al-Ahmed A, Saidur R, et al. A review on current status and challenges of inorganic phase change materials for thermal energy storage systems. Renew Sust Energ Rev. 2017;70:1072-89.
[23] Donkers PAJ, Linnow K, Pel L, Steiger M, Adan OCG. Na2SO4 center dot 10H(2)O dehydration in view of thermal storage. Chem Eng Sci. 2015;134:360-6.
[24] Kenisarin MM, Kenisarina KM. Form-stable phase change materials for thermal energy storage. Renew Sust Energ Rev. 2012;16(4):1999-2040.
[25] Ryu HW, Woo SW, Shin BC, Kim SD. Prevention of supercooling and stabilization of inorganic salt hydrates as latent heat storage materials. Sol Energy Mater Sol Cells. 1992;27(2):161-72.
[26] Oh K, Kwon S, Xu WY, Wang XJ, Toivakka M. Effect of micro- and nanofibrillated cellulose on the phase stability of sodium sulfate decahydrate based phase change material. Cellulose. 2020;27(9):5003-16.
[27] Shen Z, Kwon S, Lee HL, Toivakka M, Oh K. Enhanced thermal energy storage performance of salt hydrate phase change material: Effect of cellulose nanofibril and graphene nanoplatelet. Sol Energy Mater Sol Cells. 2021;225:11.
[28] Wang T, Wu N, Li H, Lu QL, Jiang Y. Preparation and properties of a form-stable phase-change hydrogel for thermal energy storage. J Appl Polym Sci. 2016;133(34):9.

[29] Li CC, Zhang B, Xie BS, Zhao XB, Chen J. Tailored phase change behavior of Na2SO4 center dot 10H(2)O/expanded graphite composite for thermal energy storage. Energy Convers Manage. 2020;208:13.
[30] Zohuriaan-Mehr M, Kabiri K. Superabsorbent Polymer Materials: A Review. Iran Polym J. 2008;17(6):451-77.
[31] Liu CZ, Rao ZH, Zhao JT, Huo YT, Li YM. Review on nanoencapsulated phase change materials: Preparation, characterization and heat transfer enhancement. Nano Energy. 2015;13:814-26.
[32] Alvarez-Bermudez O, Adam-Cervera I, Aguado-Hernandiz A, Landfester K, Munoz-Espi R. Magnetic Polyurethane Microcarriers from Nanoparticle-Stabilized Emulsions for Thermal Energy Storage. Acs Sustainable Chemistry & Engineering. 2020;8(49):17956-66.
[33] Purohit BK, Sistla VS. Studies on solution crystallization of Na2SO4 center dot 10H(2)O embedded in porous polyurethane foam for thermal energy storage application. Thermochim Acta. 2018;668:9-18.
[34] Zhang ZS, Lian YD, Xu XB, Xu XN, Fang GY, Gu M. Synthesis and characterization of microencapsulated sodium sulfate decahydrate as phase change energy storage materials. Appl Energy. 2019;255:11.
[35] Semsarilar M, Ladmiral V, Blanazs A, Armes SP. Cationic Polyelectrolyte-Stabilized Nanoparticles via RAFT Aqueous Dispersion Polymerization. Langmuir. 2013;29(24):7416-24.
[36] Semsarilar M, Ladmiral V, Blanazs A, Armes SP. Anionic Polyelectrolyte-Stabilized Nanoparticles via RAFT Aqueous Dispersion Polymerization. Langmuir. 2012;28(1):914-22.
[37] Yinping Z, Yi J, Yi J. A simple method, the -history method, of determining the heat of fusion, specific heat and thermal conductivity of phase-change materials. Meas Sci Technol. 1999;10(3):201-5.
[38] Goswami M, Kumar N, Li Y, Hirschey J, LaClair TJ, Akamo DO, et al. Understanding supercooling mechanism in sodium sulfate decahydrate phase-change material. J Appl Phys. 2021;129(24):245109.
[39] Li C, Zhang B, Xie B, Zhao X, Chen J. Tailored phase change behavior of Na2SO4·10H2O/expanded graphite composite for thermal energy storage. Energy Convers Manage. 2020;208:112586.
[40] Dong X, Mao JF, Geng SB, Li Y, Hou PM, Lian HL. Study on performance optimization of sodium sulfate decahydrate phase change energy storage materials. J Therm Anal Calorim. 2021;143(6):3923-34.